NANO LETTERS

pubs.acs.org/NanoLett Letter

Microwave AC Resonance Induced Phase Change in Sb_2Te_3 Nanowires

Pok Lam Tse, Fugu Tian, Laura Mugica-Sanchez, Oliver Rüger, Andreas Undisz, George Möthrath, Carsten Ronning, Susumu Takahashi, and Jia Grace Lu*

Cite This: *Nano Lett.* 2020, 20, 8668−8674

Read Online

ACCESS | Metrics & More | Article Recommendations | SI Supporting Information

ABSTRACT: Scaling information bits to ever smaller dimensions is a dominant drive for information technology (IT). Nanostructured phase change material emerges as a key player in the current green-IT endeavor with low power consumption, functional modularity, and promising scalability. In this work, we present the demonstration of microwave AC voltage induced phase change phenomenon at ~3 GHz in single Sb_2Te_3 nanowires. The resistance change by a total of 6−7 orders of magnitude is evidenced by a transition from the crystalline metallic to the amorphous semiconducting phase, which is cross-examined by temperature dependent transport measurement and high-resolution electron microscopy analysis. This discovery could potentially tailor multistate information bit encoding and electrical addressability along a single nanowire, rendering technology advancement for neuro-inspired computing devices.

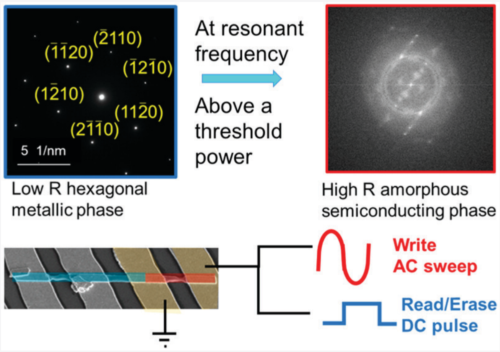

KEYWORDS: *phase change material, nanowire, AC voltage, transport measurement*

Nonvolatile memory cells with high read/write speed have been the quest in the past decades for superior performance in computing and communication electronics.[1−3] Phase change materials (PCM) have evolved into the industrial development stage when the traditional technologies decelerate. PCM demonstrates a competitive read/write speed compared to flash and embedded memories in solid state drives.[4−6] With their high speed and remarkable cycling endurance, PCM in nanostructured forms is considered as a potential replacement for storage-class memory with exceptional computing performance and reduced power consumption.

$Ge_2Sb_2Te_5$ has been extensively studied by slow passive heating and annealing[2,7] to judiciously separate out the amorphous, cubic, and hexagonal crystalline phases.[8,9] In comparison, the binary Sb_2Te_3 compound has similar phase change properties but a lower melting temperature[10] than that of $Ge_2Sb_2Te_5$. This implies reduced power requirement for information encoding and thus relieves the heating problem on an integrated device chip. In addition, Sb_2Te_3 attracts increasing research interests due to the existence of linearly dispersed surface states[11] in the band structure, which could bring new perspectives from quantum mechanics in future device designs.

Conventional operation of phase change random access memory (PCRAM) is based on the transition between the crystalline and amorphous phases, which can yield several orders of magnitude difference in the electrical resistance.[4,8,12] In such a design, applying a direct current (DC) voltage pulse in a single step to memory cells is the most common method to switch memory states.[8,13] In our work, we present alternate current (AC) voltage sweep measurements from radio frequency to microwave range on Sb_2Te_3 nanowires, which reveal a systematic stepwise increase in DC resistance at ~3 GHz above a power threshold. The samples are cross-investigated by transport measurements, as well as high-resolution electron microscopy analysis on segments with and without undergoing the AC voltage sweeps.

This unique phenomenon suggests that one can change the resistance with an AC knob tuning frequency or adjusting power level. This extra degree of freedom for memory state switching can lead to innovative developments in PCRAM for neuromorphic computation. It provides a futuristic technique to control the amount of phase change in the material, which can be utilized to obtain the optimum crystalline−amorphous ratio in order to reach a targeted resistance as an intermediate memory state. Consequently, such intermediate states pave the way to a new frame of applications of multilevel storage with a

Received: August 25, 2020
Revised: November 13, 2020
Published: November 18, 2020

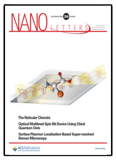

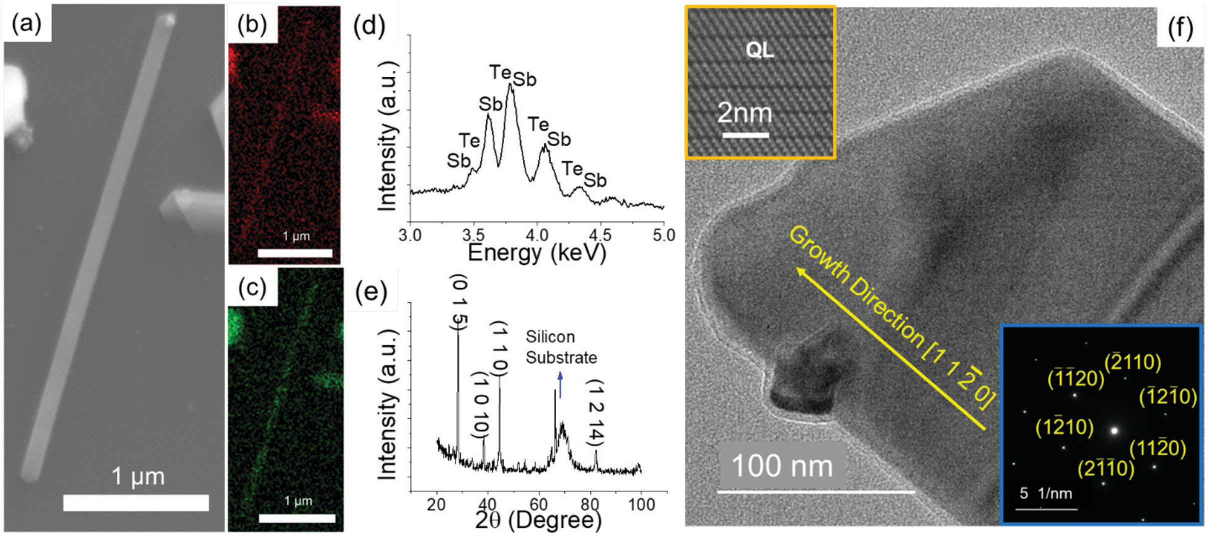

Figure 1. (a) SEM image of a Sb_2Te_3 NW on a Si/SiO_2 substrate, (b) and (c) illustrate the EDX color mappings of the respective Sb and Te elements, (d) EDX spectra, and (e) XRD spectra of Sb_2Te_3 nanowires. The peaks fit with the rhombohedral structure of Sb_2Te_3 (PDF # 00-015-0874). (f) TEM image, with lower right SAED inset showing the crystalline structure and upper left cross-section HRTEM inset displaying the stacked quintuple layers (QL).

simple device, which is very difficult to achieve with the traditional heating or application of voltage pulses.

Sb_2Te_3 has a bulk band gap of 0.28 eV and simple surface states consisting of a single Dirac cone in the band gap. The pristine crystalline structure of Sb_2Te_3 thin films and nanowires is hexagonal, and the primitive cell is rhombohedral ($R\bar{3}m$). Our previous studies on the nanowires have revealed the single crystalline structure with repeating quintuple layers of (Te−Sb−Te−Sb−Te) with an interlayer distance of 0.309 nm.[11,14−17] We have also in the past performed low-temperature magnetoresistance measurements and angle resolved photoemission spectroscopy on the nanowires synthesized by the same setup as presented in this work. The observed periodic Aharonov−Bohm type oscillations are attributed to transport in topologically protected surface states in the *p*-type Sb_2Te_3 nanowires, with a Fermi level that situates around 40 meV below the Γ- point.[11]

The scanning electron microscope (SEM) image in Figure 1a shows a single Sb_2Te_3 nanowire on a Si/SiO_2 substrate. Energy dispersive X-ray (EDX) spectroscopy mapping for Sb and Te are displayed in Figure 1b,c, respectively. The mappings of Sb and Te illustrate uniform elemental distributions along the nanowire. From the EDX spectra in Figure 1d, the atomic ratio of Sb:Te is calculated to be 2:3. Powder X-ray diffraction (XRD) (Rigaku Ultima IV diffractometer) is carried out in $\theta/2\theta$ mode with a scan speed of 4°/min. The crystal structure is confirmed to be rhombohedral (PDF # 00-015-0874), as shown in Figure 1e. A TEM image of the top view of the nanowire is displayed in Figure 1f, showing that the growth direction is along $[11\bar{2}0]$. The lower right inset depicts the corresponding selected area electron diffraction (SAED) pattern, verifying its single crystalline nature. The upper left inset of Figure 1f is the cross-section TEM image of a nanowire, manifesting the repeating quintuple layers (QL).

Three nanowire (NW) samples have been investigated at 77 K for microwave (MW) responses, with their results plotted separately in Figure 2b−d, with Figure 2a depicting the circuit diagram of one NW device on a Si/SiO_2 substrate. Clearly, the common phenomenon for all three NWs is the increase in the electrical resistance sharply around 3 GHz, independent of the geometry or material of the electrodes contacting the NWs. NW1 with Nb electrodes at 1 μm apart has an initial resistance of about 2800 Ω. Its AC sweep measurement is plotted in Figure 2b, indicating a resistance jump to 3350 Ω at 3 GHz in the first forward sweep from 10 MHz to 4 GHz. Similar results are observed in NW2 (Figure 2c) and in NW3 (Figure 2d), both fabricated with Ti/Au source and drain electrodes at 2 μm apart. It has been shown from the comparison of 2-probe and 4-probe measurement that the contact between either Nb or Ti/Au to the nanowire is of ohmic nature with negligible contact resistance (data not shown).

NW2 sample was selected for subsequent continuous backward and forward AC sweeps at a power level around −30 dBm (1 μW) after the initial forward sweep displayed in Figure 2e. For the first three sweeps shown (backward in black line, forward in red line and backward in blue line), the resistance starts to slightly increase between 2.8 and 3 GHz for both forward and backward direction. Then at the subsequent sweeps, the resistance change becomes much more pronounced when the frequency reaches 3 GHz. The final sweep spikes the resistance to a saturation level of 10^8 Ω at 3 GHz, as illustrated in the green line.

NW2 was further investigated for the resistance change by passive heating to verify that the resistance change originated from a phase change and not due to other artifacts such as oxidation or decomposition. The test results are shown in Figure S1 in the Supporting Information. The reversibility of high and low resistances in alternating short and long heating steps verifies that the sample after AC sweeps had gone through phase transition.

After the two samples (NW2 and NW3) reached the saturation levels, the resistances were measured from 77 K to room temperature. It was found that the resistances of both samples first increased and peaked at ∼100 K (as shown in Figure 3a,b), then they decreased exponentially with increasing temperature. Arrhenius semilog fittings of ln R vs $1/(k_BT)$ (where R is the DC electrical resistance, k_B is the Boltzmann constant, and T is the temperature) between 110 and 300 K

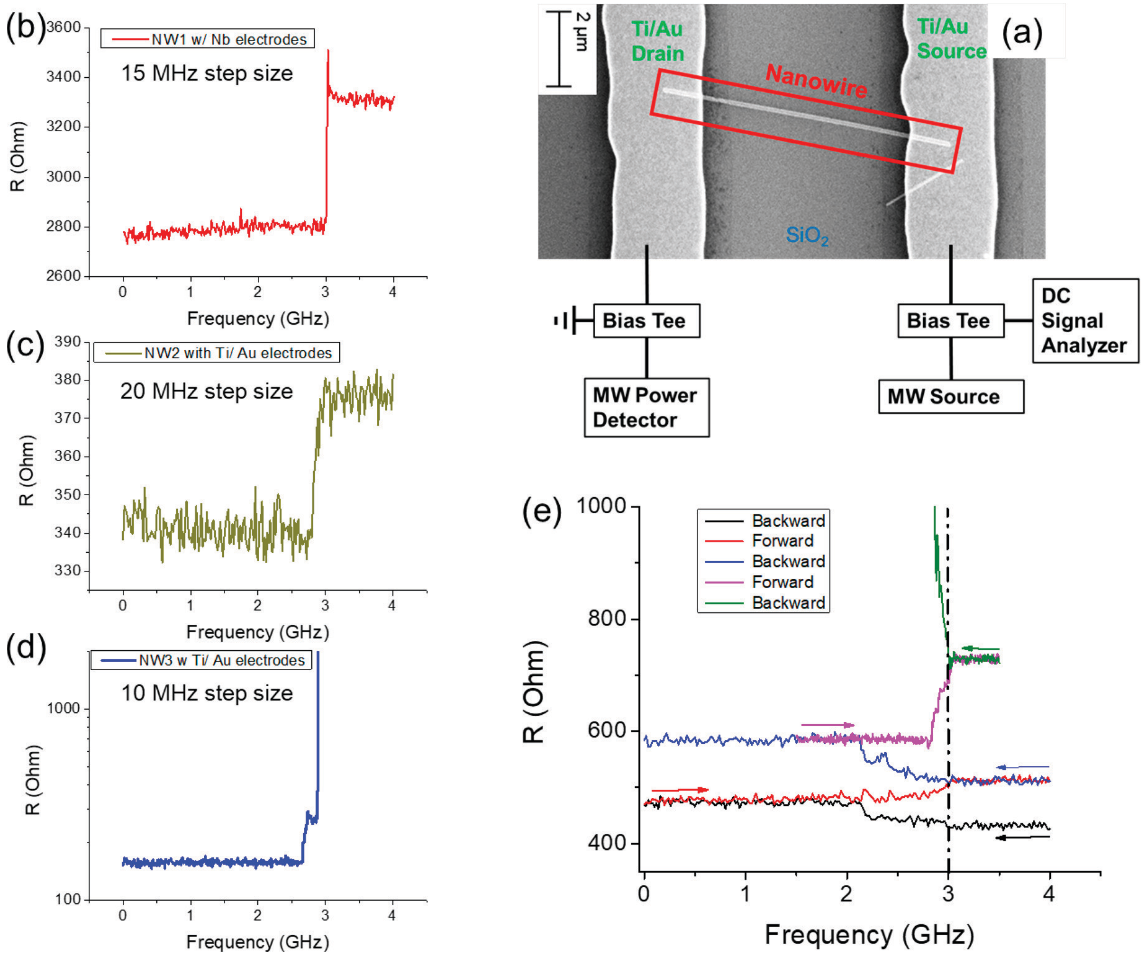

Figure 2. (a) SEM image of a contacted single Sb_2Te_3 nanowire along with the measurement circuit diagram. (b)−(d) Electrical resistance measurements at first forward AC voltage sweeps from 10 MHz to 4 GHz with 0.33 s DC integration time. Consistent increases occur at ∼3 GHz for all three NW samples. NW3 in (d) is plotted in logarithmic scale as the resistance rise at 3 GHz jumps out of the preset range of DC measurement. (e) Subsequent continuous backward and forward AC voltage sweep results for NW2 at ∼1 μW power level. The sweep directional arrows of color correspond to the data plotted by the same color.

are plotted, as shown in the insets. The results reveal that the transport is governed by thermal excitation conduction with two distinct regions between 110−220 and 220−300 K, with respective activation energy around 48 and 100 meV. These values are close to the thermal activation energies attributed to phonon-assisted hopping of small polarons, i.e., localized charges that are "self-trapped" within potential wells produced by distorting the surrounding atoms.[18] The exact transport mechanism is by itself a fascinating topic, which requires additional studies with Seebeck and Hall measurements. In contrast to NW2 and NW3 samples, the pristine reference sample NW4, which did not undertake microwave sweeps, keeps a linear relation of resistance−temperature (R−T) with $R(\Omega) \propto 0.95\ (\Omega/\mathrm{K})\cdot T\ (\mathrm{K})$, as shown in Figure 3c, manifesting a metallic behavior as in the initial state with a typical temperature coefficient estimated to be ∼0.0014/K.

The next investigation was to find out whether one can achieve segment-wise encoding along one nanowire sample, i.e., to obtain different resistance states in desired segments of one single wire. Four electrodes were fabricated across a long nanowire over 10 μm (NW5, as shown in the inset of Figure 4a). The segment of NW between contacts 2 and 3 undertook AC sweeps to get switched from the low-resistance to the high-resistance state, whereas the segment between electrodes 4 and 5 was afloat, not connected to either the DC analyzer or the MW power source. Figure 4a shows the AC sweeping results of the segment between electrodes 2 and 3 at 77 K. The first sweep at −26 dBm MW power, below the threshold power level, did not induce a resistance change at 3 GHz, whereas the second sweep at −24 dBm MW power increased the resistance sharply at 3 GHz. After continuous forward and backward sweeping at 77 K and −24 dBm, the NW reached and saturated at a high-resistance state. Additional forward and backward AC sweeps did not yield any further resistance changes (see Figure S2 in the Supporting Information). The R−T relation of this segment between electrodes 2 and 3 is plotted in Figure 4b,c upon cooling and upon warming after the AC sweeps, respectively. The linear relation during cool down indicates that the initial low-resistance state has metallic behavior, consistent with the reference NW4 sample shown in Figure 3c. After the high-resistance state is reached, the resistance decays exponentially with increasing temperature (Figure 4c). The inset in Figure 4c shows the Arrhenius semilog fitting, confirming the two ranges of thermal activation transport as that of NWs 2 and 3. In Figure S3 of Supporting Information, it shows that the segment between electrodes 4

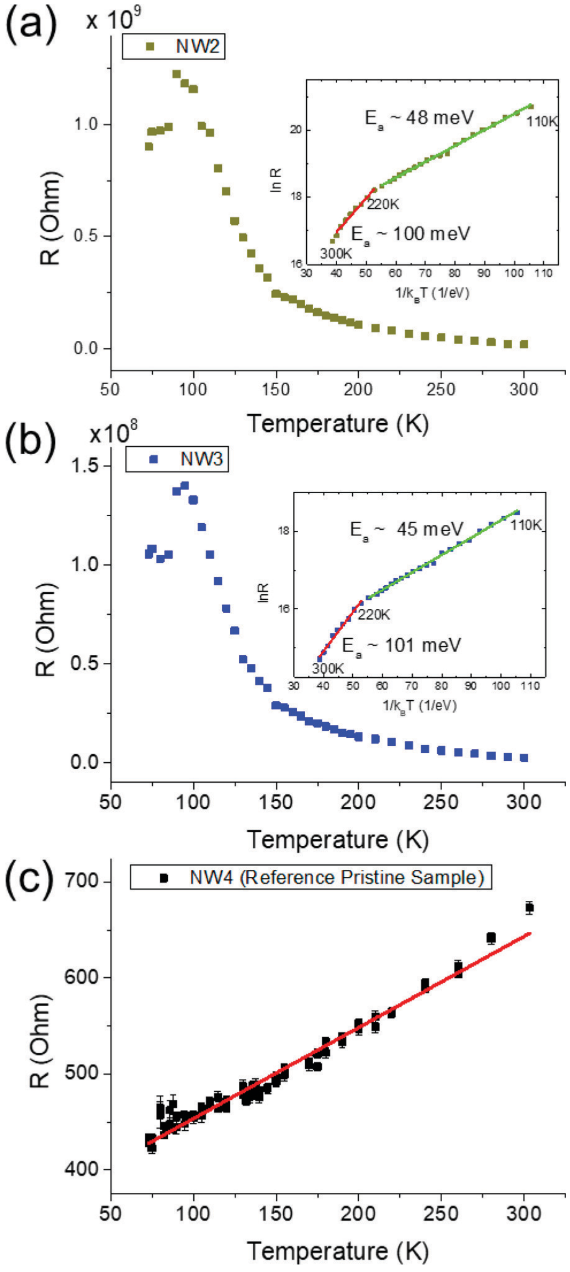

Figure 3. Temperature dependent resistance measurements during warming up from 77 to 300 K: (a) NW2 (inset: corresponding Arrhenius semilog plot with linear fittings, showing two regions of thermal activated transport); (b) NW3 (inset: corresponding Arrhenius correlation, confirming the two regions with respective activation energy of ~48 and ~100 meV); (c) NW4 reference sample with linear regression fit in red demonstrating metallic behavior.

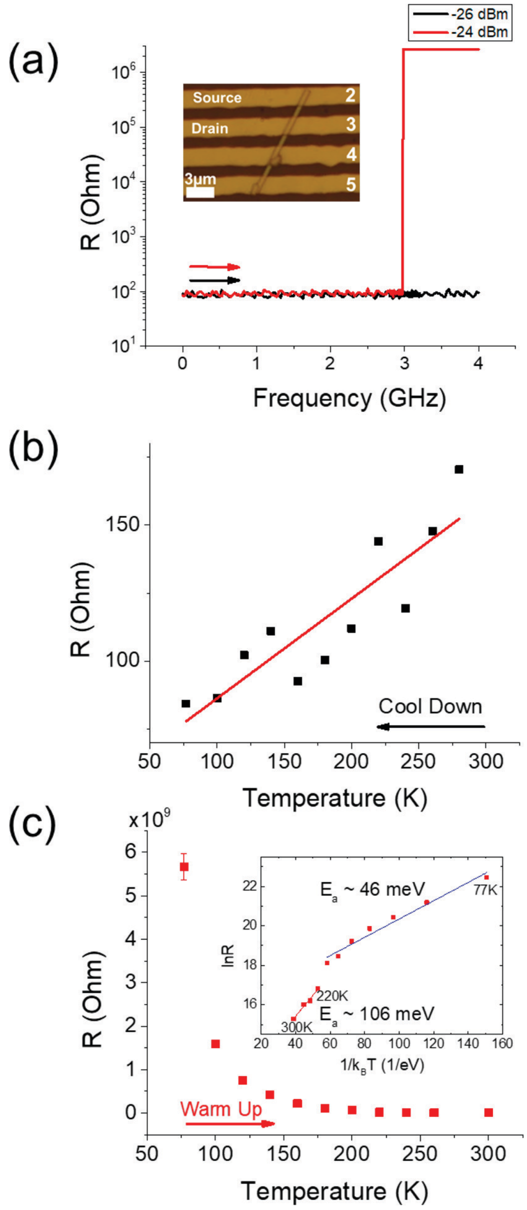

Figure 4. (a) AC voltage sweep at 77 K across electrodes 2−3 of NW5. Resistance starts to increase sharply at 3 GHz above a threshold power of −24 dBm (red line). Inset: optical image of NW5 with four electrodes. (b) *R*−*T* plot at cool down for NW segment 2−3 before AC sweeps, showing linear metallic conducting behavior. (c) *R*−*T* plot at warm up stage after MW switching to high-resistance state, showing exponential drop in resistance with increasing temperature. Inset: Arrhenius plot shows the two thermal activation regions, consistent with the results from NW2 and NW3.

and 5 in NW5 has maintained a linear *R*−*T* relation after the AC sweeps on the other segment between electrodes 2 and 3. These results demonstrate that the AC sweeps can change locally the resistance of a single nanowire, which renders a blue print of selective phase change based nanowire bit-train.

High-resolution TEM analysis on the two segments in NW5 after AC sweep was performed to examine the microstructure, as shown in Figure 5. Figure 5a shows the SEM image of the to-be-carved-out regions for cross-section TEM analysis, as indicated by yellow and blue arrows. Figure 5b shows the cross-section TEM image in the segment between contacts 2 and 3, which has been subject to AC sweeps. Panels d and f of Figure 5 are the high-resolution TEM and FFT images with hazy ring patterns, indicating that the region D is predominantly amorphous, corresponding to the high-resistance and semiconducting behavior. Region B shows the same structural features, whereas regions A and C show a layered structure, likely to be in transition to amorphous state (refer to Figure S4 in Supporting Information). In contrast, Figure 5c shows the cross-section TEM image of the segment between

https://dx.doi.org/10.1021/acs.nanolett.0c03421
Nano Lett. 2020, 20, 8668−8674

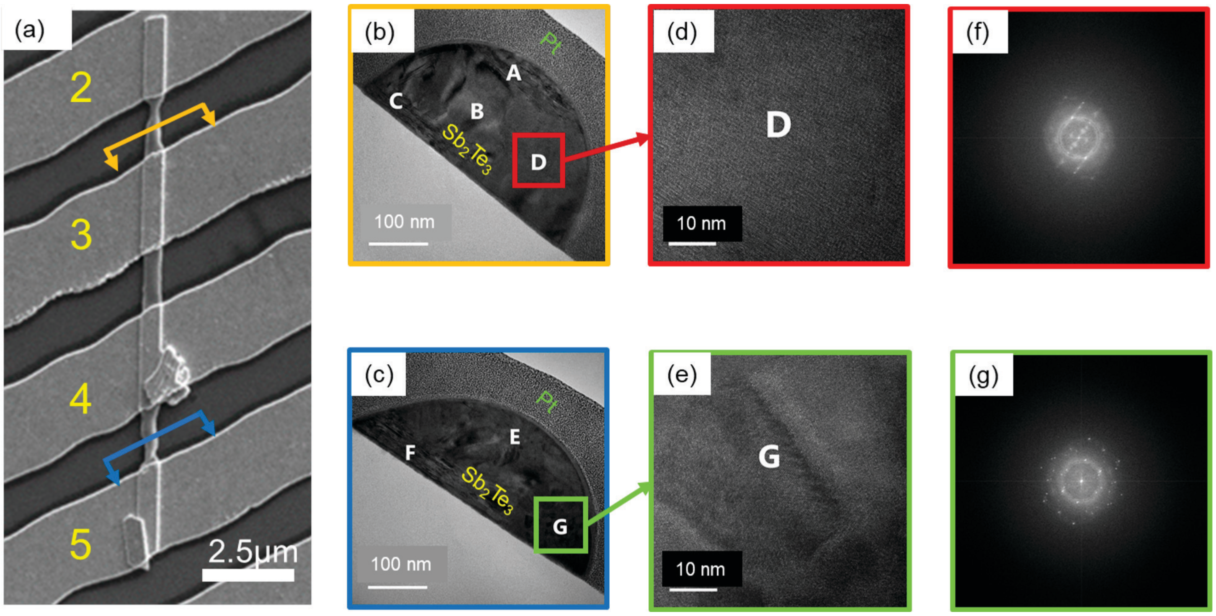

Figure 5. TEM cross-sectional analysis of NW5 after AC sweeps. (a) SEM image of NW5 after AC sweep measurements. Yellow and blue arrows indicate the segments selected for TEM cross-section imaging: between contacts 2 and 3 (underwent AC sweep) and between contacts 4 and 5 (without AC sweep). (b) TEM cross-section image of a slice of NW5 segment between contacts 2 and 3 covered by a Pt protective layer, with high-resolution TEM and FFT analysis indicating an amorphous phase, as shown in (d) and (f). (c) TEM cross-section image of a slice of NW5 segment between contacts 4 and 5 covered by a Pt protective layer, with high-resolution TEM and FFT analysis indicating a polycrystalline phase, as shown in (e) and (g).

contacts 4 and 5, which has not been subject to AC sweeps. Apart from the amorphous and layered structures respectively shown in regions E and F, region G reveals a polycrystalline structure with clear diffraction spots, as shown in the high-resolution TEM image and FFT image (Figure 5e,g). This region contributes dominantly to the low-resistance and metallic conduction behavior. Furthermore, the Sb and Te elemental composition and stoichiometry are measured by EDX in the center of NW5, and the detailed results are shown in the Supporting Information. Both segments in NW5 have similar EDX spectra (Figure S5 in Supporting Information) and the atomic ratio of Sb:Te is confirmed to be 2:3 (Figure S6), which reveals that the nanowire has minimal oxidation or composition change from the AC sweep measurements.

In brief, what we have observed are reproducible sharp increases in resistance at ~3 GHz as a result of AC sweeps on single Sb_2Te_3 nanowires. The low- to high-resistance switch by 6–7 orders of magnitude at ~77 K is accompanied by a change of metallic to semiconducting conduction characteristic, and correspondingly from crystalline to amorphous structure. At first glance, one may deduce from this evidence that the MW power at about 1 μW may have induced a phase change within the Sb_2Te_3 nanowire, via dielectric heating, comparable to that in the 2.45 GHz microwave oven since the dielectric constant of Sb_2Te_3 at 77 K is on the same order of magnitude as that of water at room temperature.[10] Based on the heat capacity equation from Pashinkin et al.,[19] a rough calculation of the energy required for a 2.5 μm long, 200 nm in radius NW segment to be heated from 77 to 403 K (130 °C) is ~0.1 nJ. Thus, the 1 μW (−30 dBm) AC voltage could easily provide enough energy to heat up and amorphize the NW. Indeed, such heating has even caused morphology changes shown in NW5 (Figure 5a). Nevertheless, this interpretation fails to address the facts that the transition occurs only at ~3 GHz, and also the phase change is concentrated locally in a segment within a wire. Furthermore, besides the resonant frequency at 3 GHz, a sufficient power level is necessary to induce a phase change. The minimum AC microwave power required for switching varies in samples from −24 to −30 dBm. This sharp transition above a power threshold further suggests an electronic transition from the low-resistance to the high-resistance state. Moreover, as frequency varies, at a constant power level above the threshold, the induced resistance jump only occurs at the resonant frequency of 3 GHz. This reinforces that the phase change is resonantly driven from an electronic nature, manifesting a different mechanism from the thermal induced phase transition.

Such sharp transitions at a resonant frequency and above a power threshold signal that the mechanism is of an electronic transition nature. Recent work on bonding calculations and simulations[20−22] suggests that the transition from the low-resistance to the high-resistance state in PCMs originates from the change of chemical bonding. Wuttig et al. has proposed a new state of matter for materials, such as Sb_2Te_3, $Ge_2Sb_2Te_5$, GeTe, etc., so-called “incipient metals”.[20,23,24] Their unique metavalent bonding goes beyond the characteristic parameters for conventional solid state bonding and possesses a bonding mechanism between those of covalency and metallicity, but at the same time, distinctly different from both. We believe that the origin of the phase transition we have observed is induced by the distortion in bonds under charge shuffling resonating at 3 GHz, such as in the metavalent bonds formed between Sb and Te layers by 5p electrons. As a result, it leads to the transition from delocalized to localized electron distributions,[25−27] rendering self-trap potential wells,[8,28] and exhibiting thermally activated transport as shown in the conductance measurements. In depth investigations are required to elucidate the nature of the atomistic bonding mechanisms.

In summary, cross-examined by charge transport and electron microscopy measurements, the reproducible resistance jump observed at 3 GHz during AC voltage sweeps is evidenced by a transition from crystalline metallic to amorphous semiconducting phase with 6−7 orders of magnitude difference in resistance. This is the first demonstration of microwave resonance induced phase change.

This new phenomenon of microwave AC voltage induced amorphization of crystalline phase change material is of fundamental interest for both experimentalists and theorists to unravel the physical nature of the phase change, especially from the perspective of bonding mechanisms. In addition, it is also unknown what role the surface states play in the phase change in the Sb_2Te_3 nanowire, which is known to have topological surface state conduction. On the other hand, this discovery could bring technology innovation for neuromorphic computing devices. Operation at room temperature is promising on the basis of our preliminary test on a nanowire sample, which shows similar results (please refer to Figure S7 in the Supporting Information). With AC frequency tuning and power level control for amorphization, along with conventional thermal or DC voltage pulse for recrystallization, one can envision potential multibit information encoding along a single nanowire, i.e., a phase change nanowire based bit train, which could have significant impact for green-IT and neuro-inspired computing devices.

ASSOCIATED CONTENT

Supporting Information

The Supporting Information is available free of charge at https://pubs.acs.org/doi/10.1021/acs.nanolett.0c03421.

> Nanowire synthesis, passive heating test, electrical measurement, structure analysis, elemental composition analysis and experimental method (PDF)

AUTHOR INFORMATION

Corresponding Author

Jia Grace Lu − *Department of Electrical and Computer Engineering - Electrophysics and Department of Physics and Astronomy, University of Southern California, Los Angeles, California 90089, United States;* orcid.org/0000-0001-9908-4061; Email: jialu@usc.edu

Authors

Pok Lam Tse − *Department of Chemical Engineering and Materials Science, University of Southern California, Los Angeles, California 90089, United States;* orcid.org/0000-0003-3832-9920

Fugu Tian − *Department of Electrical and Computer Engineering - Electrophysics, University of Southern California, Los Angeles, California 90089, United States*

Laura Mugica-Sanchez − *Department of Chemistry, University of Southern California, Los Angeles, California, CA 90089, United States*

Oliver Rüger − *Institute of Solid State Physics, Friedrich Schiller University Jena, 07743 Jena, Germany*

Andreas Undisz − *Otto Schott Institute of Materials Research, Friedrich Schiller University Jena, 07743 Jena, Germany; Institute of Materials Science and Engineering, Technische Universität Chemnitz, 09125 Chemnitz, Germany*

George Möthrath − *Department of Physics and Astronomy, University of Southern California, Los Angeles, California 90089, United States*

Carsten Ronning − *Institute of Solid State Physics, Friedrich Schiller University Jena, 07743 Jena, Germany;* orcid.org/0000-0003-2667-0611

Susumu Takahashi − *Department of Chemistry and Department of Physics and Astronomy, University of Southern California, Los Angeles, California, CA 90089, United States;* orcid.org/0000-0002-1302-2845

Complete contact information is available at: https://pubs.acs.org/10.1021/acs.nanolett.0c03421

Notes

The authors declare no competing financial interest.

ACKNOWLEDGMENTS

P.L.T. has fabricated the nanowire device samples and carried out the measurements. F.T. has significantly contributed to the analysis of the data. S.T. acknowledges supports from the National Science Foundation (DMR-1508661 and CHE-1611134 as well as CHE-2004252 with partial cofunding from the Quantum Information Science program in the Division of Physics). A.U. acknowledges support by the German Research Foundation (grant number Inst 275/391-1). We also thank Dr. Jinzhong Zhang for technical assistance of e-beam lithography and Dr. Martina Luysberg and Abdur Jalil for high-resolution TEM imaging. J.G.L. is indebted from the insightful discussions with Prof. Matthias Wuttig and Prof. Riccardo Mazzarello.

REFERENCES

(1) Yamada, N.; Ohno, E.; Nishiuchi, K.; Akahira, N.; Takao, M. Rapid-phase transitions of GeTe-Sb_2Te_3 pseudobinary amorphous thin films for an optical disk memory. *J. Appl. Phys.* **1991**, *69*, 2849.

(2) Kolobov, A.; Fons, P.; Frenkel, A.; Ankudinov, A.; Tominaga, J.; Uruga, T. Understanding the phase-change mechanism of rewritable optical media. *Nat. Mater.* **2004**, *3*, 703−8.

(3) Wuttig, M.; Yamada, N. Phase-change materials for rewriteable data storage. *Nat. Mater.* **2007**, *6*, 824−32.

(4) Wong, H. P.; Salahuddin, S. Memory leads the way to better computing. *Nat. Nanotechnol.* **2015**, *10*, 191−194.

(5) Rao, F.; Ding, K.; Zhou, Y.; Zheng, Y.; Xia, M.; Lv, S.; Song, Z.; Feng, S.; Ronneberger, I.; Mazzarello, R.; Zhang, W.; Ma, E. Reducing the stochasticity of crystal nucleation to enable subnanosecond memory writing. *Science* **2017**, *358*, 1423−1427.

(6) Zhang, W.; Mazzarello, R.; Wuttig, M.; Ma, E. Designing crystallization in phase-change materials for universal memory and neuro-inspired computing. *Nat. Rev. Mater.* **2019**, *4*, 150−168.

(7) Song, S. A.; Zhang, W.; Jeong, H.; Kim, J.; Kim, Y. In situ dynamic HR-TEM and EELS study on phase transitions of $Ge_2Sb_2Te_5$ chalcogenides. *Ultramicroscopy* **2008**, *108*, 1408−1419.

(8) Pirovano, A.; Lacaita, A. L.; Benvenuti, A.; Pellizzer, F.; Bez, R. Electronic switching in phase-change memories. *IEEE Trans. Electron Devices* **2004**, *51*, 452−459.

(9) Kato, T.; Tanaka, K. Electronic properties of amorphous and crystalline $Ge_2Sb_2Te_5$ films. *Jpn. J. Appl. Phys.* **2005**, *44*, 7340.

(10) Madelung, O.; Rossler, U.; Schulz, M. *Non-Tetrahedrally Bonded Elements and Binary Compounds;* Springer: Berlin, Heidelberg, 1998.

(11) Arango, Y. C.; Huang, L.; Chen, C.; Avila, J.; Asensio, M. C.; Grützmacher, D.; Lüth, H.; Lu, J. G.; SchäPers, T. Quantum Transport and Nano Angle-resolved Photoemission Spectroscopy on the Topological Surface States of Single Sb2Te3 Nanowires. *Sci. Rep.* **2016**, *6*, 29493.

(12) Caldwell, M. A.; Jeyasingh, R. G. D.; Wong, H. P.; Milliron, D. J. Nanoscale phase change memory materials. *Nanoscale* **2012**, *4*, 4382−4392.

(13) Kersting, B.; Salinga, M. Exploiting nanoscale effects in phase change memories. *Faraday Discuss.* **2019**, *213*, 357−370.

(14) Da Silva, J. L. F. Effective coordination concept applied for phase change $(GeTe)_m$ $(Sb_2Te_3)_n$ compounds. *J. Appl. Phys.* **2011**, *109*, No. 023502.

(15) Zheng, Y.; Xia, M.; Cheng, Y.; Rao, F.; Ding, K.; Liu, W.; Yu, J.; Song, Z.; Feng, S. Direct observation of metastable face-centered cubic Sb_2Te_3 crystal. *Nano Res.* **2016**, *9*, 3453−3462.

(16) Wang, J.; Wang, J.; Xu, Y.; Xin, T.; Song, Z.; Pohlmann, M.; Kaminski, M.; Lu, L.; Du, H.; Jia, C.; Mazzarello, R.; Wuttig, M.; Zhang, W. Layer-Switching Mechanisms in Sb_2Te_3. *Phys. Status Solidi RRL* **2019**, *13*, 1900320.

(17) Zhang, J.; Jalil, A. R.; Tse, P.; Kölzer, J.; Rosenbach, D.; Valencia, H.; Luysberg, M.; Mikulics, M.; Panaitov, G.; Grützmacher, D.; Hu, Z.; Lu, J. G.; SchäPers, T. Proximity-Effect-Induced Superconductivity in Nb/Sb_2Te_3-Nanoribbon/Nb Junctions. *Ann. Phys.* **2020**, *532*, 2000273.

(18) Baily, S. A.; Emin, D. Transport properties of amorphous antimony telluride. *Phys. Rev. B: Condens. Matter Mater. Phys.* **2006**, *73*, 165211.

(19) Pashinkin, A. S.; Malkova, A. S.; Mikhailova, M. S. The heat capacity of solid antimony telluride Sb2Te3. *Russ. J. Phys. Chem. A* **2008**, *82*, 878−879.

(20) Wuttig, M.; Deringer, V. L.; Gonze, X.; Bichara, C.; Raty, J. Incipient Metals: Functional Materials with a Unique Bonding Mechanism. *Adv. Mater.* **2018**, *30*, No. e1803777.

(21) Clima, S.; Garbin, D.; Opsomer, K.; Avasarala, N. S.; Devulder, W.; Shlyakhov, I.; Keukelier, J.; Donadio, G. L.; Witters, T.; Kundu, S.; Govoreanu, B.; Goux, L.; Detavernier, C.; Afanas'ev, V.; Kar, G. S.; Pourtois, G. Ovonic Threshold-Switching GexSey Chalcogenide Materials: Stoichiometry, Trap Nature, and Material Relaxation from First Principles. *Phys. Status Solidi RRL* **2020**, *14*, 1900672.

(22) Noé, P.; Verdy, A.; d'Acapito, F.; Dory, J.; Bernard, M.; Navarro, G.; Jager, J.; Gaudin, J.; Raty, J. Toward ultimate nonvolatile resistive memories: The mechanism behind ovonic threshold switching revealed. *Sci. Adv.* **2020**, *6*, No. eaay2830.

(23) Cheng, Y.; Cojocaru-Mirédin, O.; Keutgen, J.; Yu, Y.; KüPers, M.; Schumacher, M.; Golub, P.; Raty, J.; Dronskowski, R.; Wuttig, M. Understanding the Structure and Properties of Sesqui-Chalcogenides (i.e., V_2VI_3 or Pn_2Ch_3 (Pn = Pnictogen, Ch = Chalcogen) Compounds) from a Bonding Perspective. *Adv. Mater.* **2019**, *31*, 1904316.

(24) Kooi, B. J.; Wuttig, M. Chalcogenides by Design: Functionality through Metavalent Bonding and Confinement. *Adv. Mater.* **2020**, *32*, 1908302.

(25) Raty, J.; Schumacher, M.; Golub, P.; Deringer, V. L.; Gatti, C.; Wuttig, M. A Quantum-Mechanical Map for Bonding and Properties in Solids. *Adv. Mater.* **2019**, *31*, e1806280.

(26) Rütten, M.; Geilen, A.; Sebastian, A.; Krebs, D.; Salinga, M. Localised states and their capture characteristics in amorphous phase-change materials. *Sci. Rep.* **2019**, *9*, 6592.

(27) Jones, R. O. Bonding in phase change materials: concepts and misconceptions. *J. Phys.: Condens. Matter* **2018**, *30*, 153001.

(28) Oosthoek, J. L. M.; Krebs, D.; Salinga, M.; Gravesteijn, D. J.; Hurkx, G. A. M.; Kooi, B. J. The influence of resistance drift on measurements of the activation energy of conduction for phase-change material in random access memory line cells. *J. Appl. Phys.* **2012**, *112*, No. 084506.